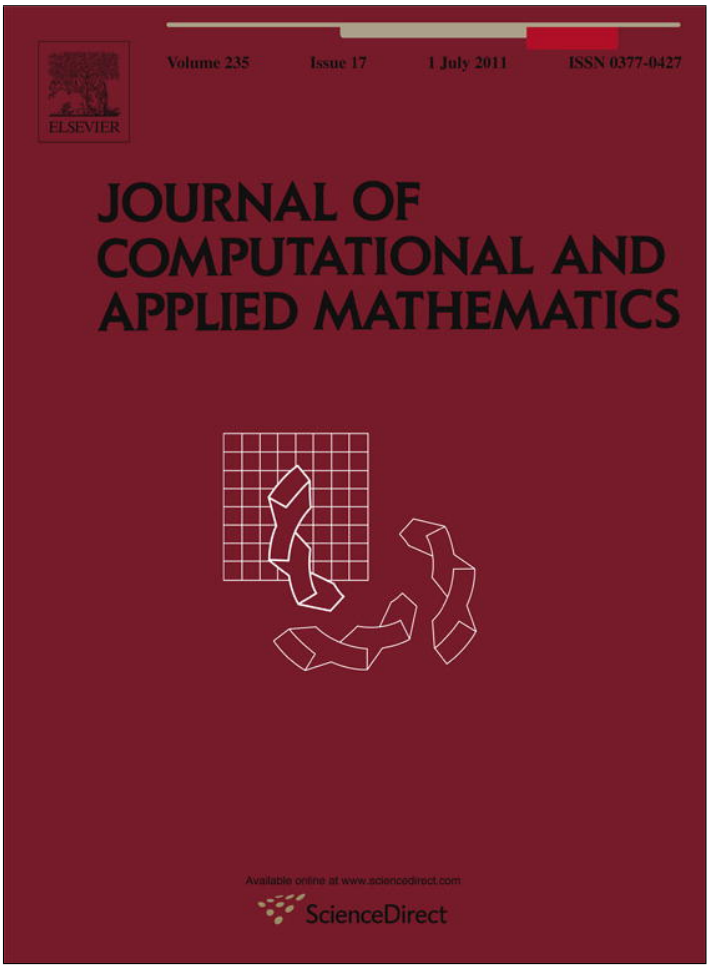

Journal of Computational and Applied Mathematics 235 (2011) 5177–5187

Contents lists available at ScienceDirect

Journal of Computational and Applied Mathematics

journal homepage: www.elsevier.com/locate/cam

Augmented high order finite volume element method for elliptic PDEs in non-smooth domains: Convergence study

Yasunori Aoki *, Hans De Sterck

Department of Applied Mathematics, University of Waterloo, Canada

ARTICLE INFO

Article history:
Received 22 September 2010
Received in revised form 23 January 2011

Keywords:
Partial differential equations
Singularity
Finite element method
Finite volume method

ABSTRACT

The accuracy of a finite element numerical approximation of the solution of a partial differential equation can be spoiled significantly by singularities. This phenomenon is especially critical for high order methods. In this paper, we show that, if the PDE is linear and the singular basis functions are homogeneous solutions of the PDE, the augmentation of the trial function space for the Finite Volume Element Method (FVEM) can be done significantly simpler than for the Finite Element Method. When the trial function space is augmented for the FVEM, all the entries in the matrix originating from the singular basis functions in the discrete form of the PDE are zero, and the singular basis functions only appear in the boundary conditions. That is to say, there is no need to integrate the singular basis functions over the elements and the sparsity of the matrix is preserved without special care. FVEM numerical convergence studies on two-dimensional triangular grids are presented using basis functions of arbitrary high order, confirming the same order of convergence for singular solutions as for smooth solutions.

1. Background

The Finite Volume Element Method (FVEM) is a numerical method for approximating the solution of a partial differential equation (PDE) in a trial function space spanned by piecewise polynomial basis functions, similar to the Finite Element Method (FEM). The coefficients of the linear combination of the basis functions are obtained by imposing the PDE through integrations over control volumes, similar to the finite volume method. Since there are many names and variations for this method, the origin of this method is not entirely clear; however, the paper in [1] is usually cited as one of the first papers on this topic. About a decade after Bank and Rose's publication, this method was extended to a quadratic method in [2]. Later Li et al. [3] and Xu and Zou [4] have carried out a convergence analysis for the quadratic method; see also [5–7]. Error estimates in the L_2 norm were given in [8]. Recently, Plexousakis and Zouraris [9] have proven a priori error estimates for the high order FVEM for one-dimensional problems (the ordinary differential equation case) with order higher than two. However, to the best of our knowledge, theoretical convergence results on the FVEM, with arbitrary order piecewise polynomial basis functions for linear elliptic problems in two-dimensional domains, are currently not yet available in the literature.

It is well known that a solution of the Poisson equation with an analytic right hand side and analytic Dirichlet boundary data is not necessarily analytic up to the boundary if the boundary is not smooth. Again, it is not easy to pin down the first discovery of such singular behaviour; we refer to the books in [10,11] for detailed discussion. The idea of augmentation of the trial function space for the finite element method (FEM) using results from regularity analysis can be found in [10] (Chapter 8.4.2) as well as in [12] (Chapter 8). Although it has been shown that the augmentation of the trial function space can recover the optimal convergence rate of the FEM, additional singular basis functions in the trial function space introduce

* Corresponding author.
E-mail address: yaoki@uwaterloo.ca (Y. Aoki).

0377-0427/$ – see front matter © 2011 Elsevier B.V. All rights reserved.
doi:10.1016/j.cam.2011.05.004

complications. Integration of the singular basis function must be done analytically or using special quadrature rules, and special care is needed to preserve the sparsity of the stiffness matrix.

Error estimates for the first order FVEM for elliptic PDEs with a derivative blow-up singularity in a non-convex domain are presented in [13]. They show that the rate of error convergence decreases when a singularity is present. Djadel et al. [14] have employed a grid refinement technique, similar to what is presented in Chapter 8.4.1 of [10], for the first order FVEM to improve the rate of convergence. On the other hand, to the best of our knowledge, augmentation of the trial function space has not been studied for the FVEM.

In this paper, we demonstrate the augmentation of the trial function space for the arbitrary high order FVEM by presenting numerical convergence studies for the Poisson equation with derivative blow-up singularity at a reentrant corner. We first perform a numerical convergence study of the FVEM with arbitrary order piecewise polynomial basis functions on triangular grids for non-singular solutions using the systematic way to construct control volumes that was proposed in [15], and that is a generalization of second order approaches in [2–4]; see also [16–18]. Well-posedness of the FVEM on triangular grids for this particular way of constructing the control volumes was proved for second order methods in [4] under certain conditions on the angles of the triangular elements. For orders higher than two, it can be observed that H^1 convergence orders are the same as the optimal orders exhibited by the Galerkin FEM, but that L_2 convergence order is sub-optimal for polynomials of even order, similar to what has been observed before for the Discontinuous Galerkin method [19–21] and for the one-dimensional FVEM [9] (see also [18]). We then show numerically that the presence of a derivative blow-up singularity at a reentrant corner can pollute the numerical solution and the rate of convergence. Finally, we show numerically how the rate of convergence can be recovered by augmentation of the trial function space, leading to an elegant and efficient augmented high order FVEM.

The rest of this paper is organized as follows. Section 2 discusses model problems, and Section 3 presents the numerical method indicating the choice of control volumes and the augmentation approach. Section 4 gives numerical results and Section 5 concludes the paper.

2. Model problems

In this paper, we consider the Poisson equation with Dirichlet boundary condition

$$\Delta u = f(x, y) \quad \text{in } \Omega, \tag{1}$$

$$u = g(x, y) \quad \text{on } \partial\Omega, \tag{2}$$

where $\Omega \subset \mathbb{R}^2$ is an open polygonal domain with a finite number of vertices, $\partial\Omega$ is the boundary of the polygonal domain, $f(x, y)$ is a function in $L^2(\Omega) \cap C^0(\Omega)$ and $g(x, y)$ is a function in $H^2(\partial\Omega)$. Note that, for simplicity, we only consider classical solutions of the PDE in this paper ($f \in C^0(\Omega)$). The FVEM can also be used to approximate non-classical solutions (see [1]).

2.1. Regularity of solutions of the Poisson problem

Since a polygonal domain is a Lipschitz domain, showing the existence and the interior smoothness of the solution of boundary value problem (BVP), (1)–(2) is straightforward. It can be proven by the Lax–Milgram theorem that there exists a unique solution $u \in H^1(\Omega)$ of BVP (1)–(2) (See Lemma 4.4.3.1 of [10]). Also, it is known that boundary derivative blow-up singularities can occur at the vertices of the domain. We now give a known regularity result for the solution at the vertices.

Let $(x_{s_i}, y_{s_i}) \in \partial\Omega$ be the vertices with singularities of the boundary of domain Ω, and let N_{vert} be the number of vertices with singularities. For each vertex (x_{s_i}, y_{s_i}), local polar coordinates r_i and θ_i are defined as depicted in Fig. 1. Define the interior angle α_i for each vertex (x_{s_i}, y_{s_i}) so that $(r_i, \theta_i) \in \Omega$ if $0 < \theta_i < \alpha_i$ for sufficiently small $r_i > 0$. Using the above notation, the modified shift theorem can be stated as follows.

Theorem 2.1 (*Modified Shift Theorem*). *Let $u(x, y)$ be the solution of boundary value problem (1)–(2). Then for all $m \in \mathbb{N}$, there exist constants $k_{i,j} \in \mathbb{R}$ such that*

$$u(x, y) - \sum_{0<\lambda_{i,j}<m+1} k_{i,j}\psi_{i,j} \in H^{m+1}(\Omega), \tag{3}$$

where

$$\psi_{i,j} = \begin{cases} r_i^{\lambda_{i,j}} \sin(\lambda_{i,j}\theta_i) & \text{if } \lambda_{i,j} \notin \mathbb{Z}, \\ r_i^{\lambda_{i,j}} \left\{\ln r_i \sin(\lambda_{i,j}\theta_i) + \theta_i \cos(\lambda_{i,j}\theta_i)\right\} & \text{if } \lambda_{i,j} \in \mathbb{Z}, \end{cases} \tag{4}$$

with

$$\lambda_{i,j} = j\pi/\alpha_i. \tag{5}$$

This theorem is a direct implication of Theorem 5.1.3.5 in Grisvard [10].

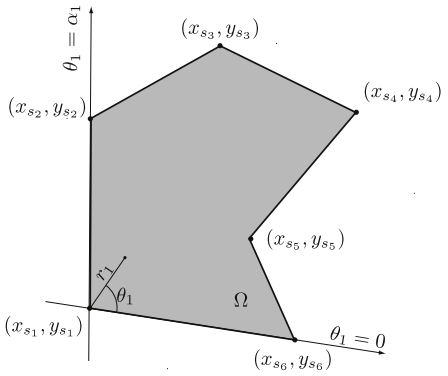

Fig. 1. Example of a polygonal domain and the local polar coordinates for $i = 1$.

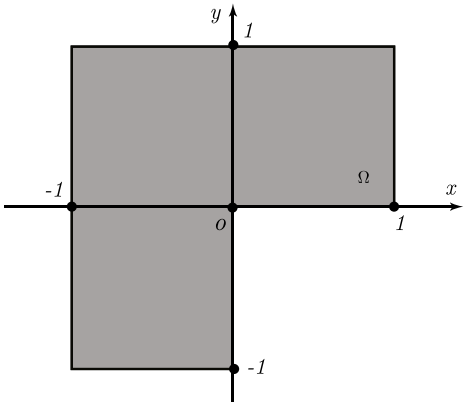

Fig. 2. L-shaped domain.

In order to illustrate the augmentation of the trial function space, we consider the following model problems.

2.2. Model Problem 1

Consider Poisson problem (1)–(2) with the following right hand side and boundary data:

$$f(x, y) = 20\,x^3y^4 + 12\,x^5y^2 \quad \text{in } \Omega, \tag{6}$$

$$g(x, y) = x^5y^4 \quad \text{on } \partial\Omega, \tag{7}$$

where domain Ω is a unit square domain. The exact solution is

$$u(x, y) = x^5y^4 \quad \text{in } \Omega. \tag{8}$$

2.3. Model Problem 2

Consider Poisson problem (1)–(2) with the following right hand side and boundary data:

$$f(x, y) = 20\,x^3y^4 + 12\,x^5y^2 \quad \text{in } \Omega, \tag{9}$$

$$\begin{aligned} g(x, y) \;=\; & x^5y^4 + 2\,r^{\frac{2}{3}} \sin\left(\frac{2}{3}\theta\right) + 7\,r^{\frac{4}{3}} \sin\left(\frac{4}{3}\theta\right) + r^2\{\ln r \sin(2\theta) + \theta\cos(2\theta)\} \\ & + 8\,r^{\frac{8}{3}} \sin\left(\frac{8}{3}\theta\right) + 2\,r^{\frac{10}{3}} \sin\left(\frac{10}{3}\theta\right) + 8\,r^4\{\ln r \sin(4\theta) + \theta\cos(4\theta)\} \quad \text{on } \partial\Omega, \end{aligned} \tag{10}$$

where domain Ω is as illustrated in Fig. 2, and r and θ are polar coordinates centred at the origin. The exact solution is

$$\begin{aligned} u(x, y) \;=\; & x^5y^4 + 2\,r^{\frac{2}{3}} \sin\left(\frac{2}{3}\theta\right) + 7\,r^{\frac{4}{3}} \sin\left(\frac{4}{3}\theta\right) + r^2\{\ln r \sin(2\theta) + \theta\cos(2\theta)\} \\ & + 8\,r^{\frac{8}{3}} \sin\left(\frac{8}{3}\theta\right) + 2\,r^{\frac{10}{3}} \sin\left(\frac{10}{3}\theta\right) + 8\,r^4\{\ln r \sin(4\theta) + \theta\cos(4\theta)\} \quad \text{in } \Omega. \end{aligned} \tag{11}$$

Note that the r-directional derivative of $u(x, y)$ blows up at the origin, but $g(x, y)$ is analytic on $\partial\Omega$ since $g(x, 0) = 0$ and $g(0, y) = (-3/2\,y^2 + 12\,y^4)\pi$.

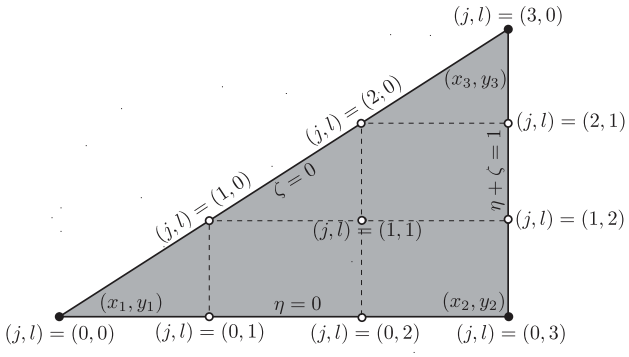

Fig. 3. Placement of nodes in an element triangle ($p = 3$).

3. Numerical method

The FVEM approximates the solution of a BVP in a finite-dimensional trial function space by integrating the PDE over a finite number of control volumes. In this section, our construction of shape functions and control volumes is explained. Then, using the shape functions and the control volumes, the FVEM is built up using both a standard trial function space and an augmented trial function space.

3.1. Shape functions

To approximate the solution of BVP (1)–(2), a finite-dimensional trial function space $S_p^h \subset H^1(\Omega)$ needs to be constructed. Similarly to the FEM, pth order piecewise polynomial shape functions are used to form a basis of the trial function space. We construct the shape functions the same way as the FEM, as briefly described in the following. (See standard textbooks on the FEM, e.g., [22], for a more detailed discussion.)

Finite element triangulation of the domain

First, a set of triangular open subdomains of Ω denoted by $\{T_1, T_2, \ldots, T_{N_e}\}$ is chosen in such a way that

$$T_i \cap T_j = \emptyset \quad \text{if } i \neq j, \tag{12}$$

$$\bigcup_{i=1,\ldots,N_e} \bar{T}_i = \bar{\Omega}, \tag{13}$$

and no vertex of any triangle lies in the interior of an edge of another triangle [22]. We shall refer to these triangles as *element triangles*, with N_e denoting the number of element triangles. We let h be the maximum diameter of the element triangles and use it to quantitatively describe the resolution of the triangular mesh. The parameter h will be used in the convergence study of Section 4.

Node placement in the finite elements

In order to construct nodal basis functions, we now choose the location of nodes for each element triangle. Consider the element triangle T_i, and let $\{(x_1, y_1), (x_2, y_2), (x_3, y_3)\}$ be the vertices of this element triangle. The $(x, y) \in \bar{T}_i$ are defined by

$$x = (1 - \zeta - \eta)\, x_1 + \zeta\, x_2 + \eta\, x_3 \quad \text{for } 0 \leq \zeta + \eta \leq 1 \text{ and } \eta, \zeta \geq 0, \tag{14}$$

$$y = (1 - \zeta - \eta)\, y_1 + \zeta\, y_2 + \eta\, y_3 \quad \text{for } 0 \leq \zeta + \eta \leq 1 \text{ and } \eta, \zeta \geq 0. \tag{15}$$

We wish to construct a pth order polynomial in $\bar{T}_i$ using a linear combination of nodal basis functions. Hence, we require the same number of nodes in $\bar{T}_i$ as the degrees of freedom of a pth order polynomial, i.e., $(p + 1)(p + 2)/2$. We define the coordinate of each node by choosing η and ζ as in the following (also depicted in Fig. 3):

$$\eta = \frac{j}{p}, \qquad \zeta = \frac{l}{p}, \tag{16}$$

where

$$j, l = 0, 1, 2, \ldots, p, \tag{17}$$

$$j + l \leq p. \tag{18}$$

We let N_{node} be the total number of distinct nodes on the whole mesh and denote the location of these nodes by (x_i, y_i) for $i = 1, 2, \ldots, N_{node}$. Note that on the uniform grids we are considering in this paper, the total number of distinct nodes

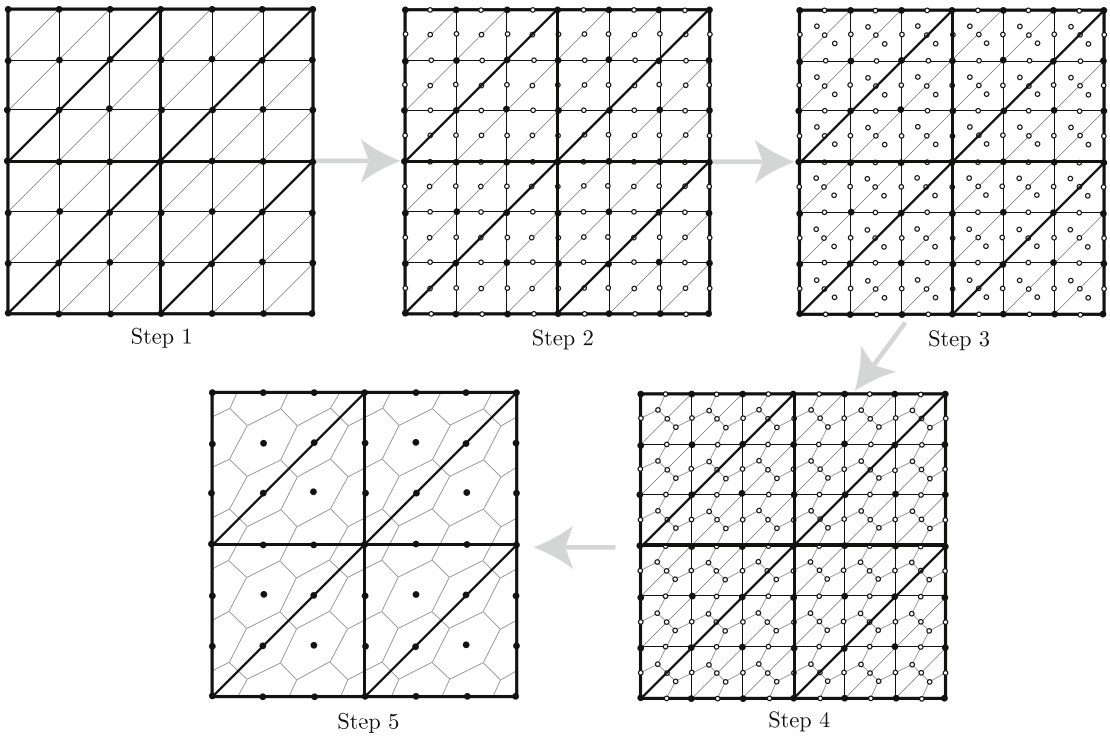

Fig. 4. Construction of the control volumes for eight element triangles ($p = 3$).

is $O(1/h^2)$. Let $\mathcal{N}$ be the set of node indices $\{1, 2, 3, \ldots, N_{node}\}$, and $\mathcal{N}_{int}$ and $\mathcal{N}_{bound}$ be disjoint subsets of $\mathcal{N}$ denoting the nodes in the interior and on the boundary of the domain, respectively, i.e.,

$$(x_i, y_i) \in \Omega^o \quad \forall i \in \mathcal{N}_{int}, \tag{19}$$

$$(x_i, y_i) \in \partial\Omega \quad \forall i \in \mathcal{N}_{bound}, \tag{20}$$

$$\mathcal{N}_{int} \cup \mathcal{N}_{bound} = \mathcal{N}. \tag{21}$$

We denote the number of nodes in sets $\mathcal{N}_{int}$ and $\mathcal{N}_{bound}$ by N_{int} and N_{bound}. In addition, we let $\mathcal{T}_i$ be the index set of all element triangles that contain node i in their closure.

Shape functions

We now construct a shape function $\phi_i(x, y)$ for each node with $\phi_i(x, y)$ pth order piecewise polynomial in Ω and pth order polynomial in T_j for all $j = 1, \ldots, N_e$, and with $\phi_i(x_j, y_j) = \delta_{i,j}$. It can be shown that $\phi_i(x, y) \in C^0(\Omega)$ and the set $\{\phi_1, \phi_2, \ldots, \phi_{N_{node}}\}$ is linearly independent. In addition, we note that $\cup_{j\in\mathcal{T}_i} \bar{T}_j$ is the support of the shape function ϕ_i.

3.2. Control volumes

We divide the domain Ω into a finite number of subdomains for finite volume integration. We follow the specific approach for constructing the control volumes for second order polynomials on triangles of Liebau [2] ([4] proves the inf–sup condition and convergence for, among others, this choice of control volumes, under certain conditions on the element angles; see also [6]), and we extend it to arbitrary high order in the same way as proposed in [15]. The subdomains are chosen so that the union of the closure of the subdomains is the closure of the domain, and the closure of each subdomain contains exactly one finite element node. We construct the subdomains by the following five steps (with each step depicted in Fig. 4):

Step 1: Subdivide the element triangles in smaller triangles in a regular fashion, using the finite element nodes (see Fig. 4).
Step 2: Determine the midpoint of each edge of the small triangles.
Step 3: Determine the centroids of the small triangles.
Step 4: Connect midpoints with centroids by line segments.
Step 5: Divide the domain Ω into N_{node} polygonal open subdomains enclosed by the line segments created in Step 4.

We shall refer to these polygonal open subdomains of Ω as *control volumes*. The control volume associated with the node at (x_i, y_i) is denoted as Ω_i.

3.3. FVEM with standard trial function space

We now formulate the discrete form of the boundary value problem. We first construct the standard trial function space using the shape functions and then discretize the PDE using the control volumes.

Standard trial function space

We construct a finite-dimensional function space S_p^h with the pth order piecewise polynomial shape functions described in Section 3.1:

$$S_p^h := span\{\phi_1, \phi_2, \ldots, \phi_{N_{node}}\}. \tag{22}$$

We approximate the solution of the boundary value problem by a linear combination of the shape functions ϕ_i in S_p^h, the standard trial function space of our FVEM, i.e.,

$$u \approx u^h := \sum_{i=1}^{N_{node}} c_i \phi_i, \tag{23}$$

where $c_i \in \mathbb{R}$. We note that $S_p^h \subset W_1^2(\Omega) \subset H^1(\Omega)$.

Discrete integral form

The discrete integral form of PDE (1) can be motivated as follows. Since f is continuous in Ω, PDE (1) is equivalent to the following equation:

$$\int_{\Omega_\alpha} \Delta u \, dA = \int_{\Omega_\alpha} f \, dA \quad \text{for all open subdomains } \Omega_\alpha \subset \Omega. \tag{24}$$

Applying the divergence theorem, we obtain

$$\int_{\partial\Omega_\alpha} \nu \cdot \nabla u \, ds = \int_{\Omega_\alpha} f \, dA \quad \text{for all open subdomains } \Omega_\alpha \subset \Omega, \tag{25}$$

where ν is the unit outward normal vector on the boundary $\partial\Omega_\alpha$. We now approximate u by u^h and impose Eq. (25) on the control volumes Ω_i associated with the interior nodes, and obtain

$$\sum_{j=1}^{N_{node}} c_j \int_{\partial\Omega_i} \nu \cdot \nabla\phi_j \, ds = \int_{\Omega_i} f \, dA \quad \forall i \in \mathcal{N}_{int}, \tag{26}$$

where ν is the unit outward normal vector on the boundary of the control volume $\partial\Omega_i$. Note that $\nabla\phi_j$ in Eq. (26) is well defined at all Gauss points for all $i \in \mathcal{N}_{int}$.

Boundary conditions

Now consider boundary conditions (BCs) so that u^h satisfies BC (2) exactly at each boundary node, i.e.,

$$u^h(x_i, y_i) = \sum_{j=1}^{N_{node}} c_j\phi_j(x_i, y_i) = c_i = g(x_i, y_i) \quad \forall i \in \mathcal{N}_{bound}. \tag{27}$$

This provides N_{bound} additional conditions which, together with the N_{int} equations of (26), fully specify the $N_{node} = N_{int} + N_{bound}$ unknown coefficients in linear combination (23).

FVEM with standard trial function space

The FVEM with the standard trial function space is thus given by:

Find $\{c_1, c_2, \ldots, c_{N_{node}}\}$ such that

$$\sum_{j=1}^{N_{node}} c_j \int_{\partial\Omega_i} \nu \cdot \nabla\phi_j \, ds = \int_{\Omega_i} f \, dA \quad \forall i \in \mathcal{N}_{int}, \tag{28}$$

$$c_i = g(x_i, y_i) \quad \forall i \in \mathcal{N}_{bound}. \tag{29}$$

We solve the system of Eqs. (28) and (29) by solving a matrix equation of the form $A \cdot \boldsymbol{x} = \boldsymbol{b}$ where A is a $N_{node} \times N_{node}$ matrix and $\boldsymbol{x}$ and $\boldsymbol{b}$ are vectors of length N_{node}. By rearranging the nodal indices so that

$$\mathcal{N}_{int} = \{1, 2, \ldots, N_{int}\}, \tag{30}$$

$$\mathcal{N}_{bound} = \{N_{int} + 1, N_{int} + 2, \ldots, N_{node}\}, \tag{31}$$

we obtain the matrix equation

$$\left[\begin{array}{c|c} A_{11} & A_{12} \\ \hline 0 & I \end{array}\right] \cdot \left[\begin{array}{c} \boldsymbol{x}_1 \\ \hline \boldsymbol{x}_2 \end{array}\right] = \left[\begin{array}{c} \boldsymbol{b}_1 \\ \hline \boldsymbol{b}_2 \end{array}\right] \tag{32}$$

where

the ith row, jth column of the $N_{int} \times N_{node}$ matrix $[A_{11}\, A_{12}]$ is given by $\int_{\partial\Omega_i} \nu \cdot \nabla\phi_j \, ds$,
the ith element of vector $[\boldsymbol{x}_1^T \boldsymbol{x}_2^T]^T$ is c_i,
the ith element of vector $\boldsymbol{b}_1$ is $\int_{\Omega_i} f \, dA$,
and the ith element of vector $\boldsymbol{b}_2$ is $g(x_{N_{int}+i}, y_{N_{int}+i})$.

Since the support of ϕ_j is $\cup_{k\in\mathcal{T}_j} \bar{T}_k$, the ith row, jth column of the matrix $[A_{11}\, A_{12}]$ is 0 if $\Omega_i \cap \left(\cup_{k\in\mathcal{T}_j} \bar{T}_k\right) = \emptyset$. Also, the number of non-zero elements of each row of the matrix $[A_{11}A_{12}]$ only depends on p. Hence the number of non-zeros of matrix A is $O(N_{node}) = O(1/h^2)$.

We shall refer to this approximation technique for the solution of the BVP with pth order piecewise polynomials as the pth *order FVEM*.

3.4. FVEM with augmented trial function space

The FVEM with an augmented trial function space can be formulated following similar steps to what was presented in Section 3.3. In this section, we describe the steps with special emphasis on how they avoid the integration of singular basis functions and preserve the sparsity of the matrix system. For simplicity, we assume there only exists one corner singularity (i.e., $N_{vert} = 1$). Extension to multiple points of singularity can be implemented easily. Due to our construction of the mesh and nodes, there is always a node at a point of singularity. We denote the location of the singularity by (x_s, y_s) (i.e., we let the index of the singular node be s).

Augmented trial function space

In addition to the basis functions in the standard trial function space, we include the $\psi_{1,j}$ defined in Eq. (4) in the basis of the trial function space. That is to say, the augmented trial function space $\hat{S}_p^h$ is defined as

$$\hat{S}_p^h := span\{\phi_1, \phi_2, \ldots, \phi_{N_{node}}, \psi_{1,1}, \psi_{1,2}, \ldots, \psi_{1,N_s}\}, \tag{33}$$

where N_s is the number of singular basis functions, which can be chosen according to Theorem 2.1 and the theory of polynomial interpolation. In our implementation, we choose $N_s = 2(p+1) - 1$ to guarantee that the solution is in H^{p+1} after subtracting a suitable linear combination of the singular basis functions, for any polygonal domain. It is beneficial to choose the $\psi_{1,j}$ as the singular basis functions, since they are harmonic functions (i.e., $\Delta\psi_{1,j} = 0$) which leads to significant simplifications in the linear equations, see below. Similarly to Eq. (23) we approximate u by $\hat{u}^h$ such that

$$u \approx \hat{u}^h := \sum_{i=1}^{N_{node}} c_i \phi_i + \sum_{i=1}^{N_s} k_i \psi_{1,i}, \tag{34}$$

where $c_i, k_i \in \mathbb{R}$. We note that $S_p^h \subsetneq \hat{S}_p^h$. The first few singular basis functions for Model Problem 2 are listed below:

$$\psi_{1,1} = r^{\frac{2}{3}} \sin\left(\frac{2}{3}\theta\right), \tag{35}$$

$$\psi_{1,2} = r^{\frac{4}{3}} \sin\left(\frac{4}{3}\theta\right), \tag{36}$$

$$\psi_{1,3} = r^2\{\ln r \sin(2\theta) + \theta\cos(2\theta)\}, \tag{37}$$

$$\vdots$$

Discrete integral form

Following Eq. (25), the discrete integral form can be written as

$$\sum_{j=1}^{N_{node}} c_j \int_{\partial\Omega_i} \nu \cdot \nabla\phi_j \, ds + \sum_{j=1}^{N_s} k_j \int_{\partial\Omega_i} \nu \cdot \nabla\psi_{1,j} \, ds = \int_{\Omega_i} f \, dA \quad \forall i \in \mathcal{N}_{int}. \tag{38}$$

By applying the divergence theorem, it can easily be seen that, for the singular basis functions $\psi_{1,j}$, it holds that

$$\int_{\Omega_i} \Delta\psi_{1,j} \, dA = \int_{\partial\Omega_i} \nu \cdot \nabla\psi_{1,j} \, ds = 0 \quad \forall i \in \mathcal{N}_{int}, \tag{39}$$

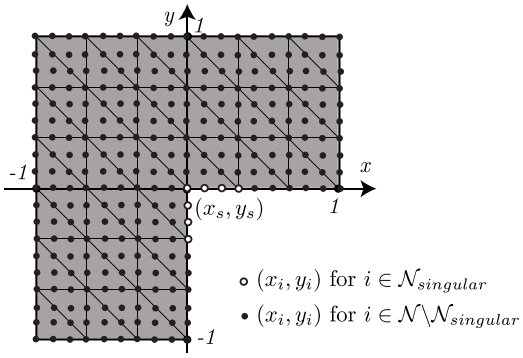

Fig. 5. Placement of $\mathcal{N}_{singular}$ ($p = 3$, $N_e = 54$).

which means that Eq. (38) can be simplified to

$$\sum_{j=1}^{N_{node}} c_j \int_{\partial\Omega_i} \nu \cdot \nabla\phi_j \, \mathrm{d}s = \int_{\Omega_i} f \, \mathrm{d}A \quad \forall i \in \mathcal{N}_{int}, \tag{40}$$

which, surprisingly, is the same as Eq. (26), i.e., the singular basis functions do not lead to extra terms in the equations for the interior nodes.

Boundary conditions

Now consider the BCs so that $\hat{u}^h$ satisfies BC (2) exactly at each boundary node, i.e.,

$$\hat{u}^h(x_i, y_i) = \sum_{j=1}^{N_{node}} c_j \phi_j(x_i, y_i) + \sum_{j=1}^{N_s} k_j \psi_{1,j}(x_i, y_i) = g(x_i, y_i) \quad \forall i \in \mathcal{N}_{bound}. \tag{41}$$

With $\phi_j(x_i, y_i) = \delta_{i,j}$, Eq. (41) can be simplified as

$$c_i + \sum_{j=1}^{N_s} k_j \psi_{1,j}(x_i, y_i) = g(x_i, y_i) \quad \forall i \in \mathcal{N}_{bound}. \tag{42}$$

Thus, we see that the singular basis functions only appear in the boundary conditions. Also, to impose the boundary conditions there is no need for integrating the singular basis functions.

FVEM with augmented trial function space

We finally combine Eqs. (40) and (42) to formulate the FVEM. We have $N_{int} + N_{bound}$ equations for $N_{int} + N_{bound} + N_s$ unknowns, which is an underdetermined problem. Since we need N_s additional conditions, we make the natural choice of additionally imposing the integral form (40) for the control volumes Ω_i of the N_s boundary nodes that are closest to the point of singularity. Note that, in these integrals, the gradients on the control volume edges that are part of the domain boundary are to be evaluated in the limiting sense from the inside of the control volume.

Combining these equations, we seek $\{c_j\}_{j=1}^{N_{node}}$, $\{k_j\}_{j=1}^{s}$ satisfying

$$\sum_{j=1}^{N_{node}} c_j \int_{\partial\Omega_i} \nu \cdot \nabla\phi_j \, \mathrm{d}s = \int_{\Omega_i} f \, \mathrm{d}A \quad \forall i \in \mathcal{N}_{int} \cup \mathcal{N}_{singular}, \tag{43}$$

$$c_i + \sum_{j=1}^{N_s} k_j \psi_{1,j}(x_i, y_i) = g(x_i, y_i) \quad \forall i \in \mathcal{N}_{bound}, \tag{44}$$

where $\mathcal{N}_{singular}$ is the set of indices of the N_s boundary nodes closest to the point of singularity, chosen as depicted in Fig. 5. The matrix equation $\hat{A}\hat{x} = \hat{b}$ corresponding to Eqs. (43)–(44) can be depicted as

$$\left[\begin{array}{cc|c} A_{11} & A_{12} & 0 \\ 0 & I & A_{23} \\ \hline A_{31} & A_{32} & 0 \end{array}\right] \cdot \left[\begin{array}{c} \boldsymbol{x}_1 \\ \boldsymbol{x}_2 \\ \hline \boldsymbol{x}_3 \end{array}\right] = \left[\begin{array}{c} \boldsymbol{b}_1 \\ \boldsymbol{b}_2 \\ \hline \boldsymbol{b}_3 \end{array}\right] \tag{45}$$

where matrices A_{11}, A_{12} and vectors $\boldsymbol{x}_1$, $\boldsymbol{x}_2$, $\boldsymbol{b}_1$ and $\boldsymbol{b}_2$ are exactly as in (32), and

the jth column of the $N_s \times N_{node}$ matrix $[A_{31}\, A_{32}]$ is $\int_{\partial\Omega_i} \nu \cdot \nabla\phi_j \, ds$ for $i \in \mathcal{N}_{singular}$,
the ith row, jth column of the $N_{bound} \times N_s$ matrix A_{23} is $\psi_{1,j}(x_{N_{int}+i}, y_{N_{int}+i})$,

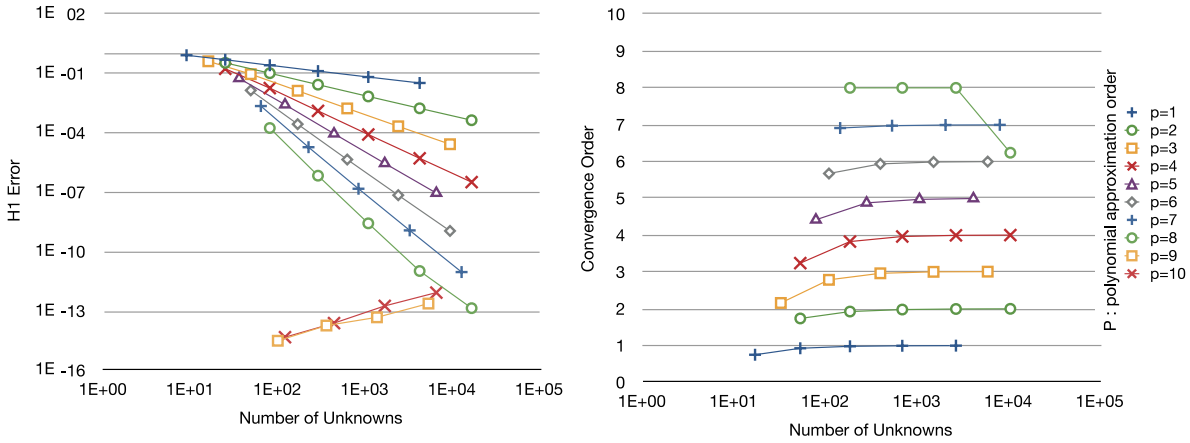

Fig. 6. H^1 error convergence for the Poisson problem with 9th order polynomial exact solution (Model Problem 1).

the ith element of vector $\boldsymbol{x}_3$ is k_i,
and the elements of vector $\boldsymbol{b}_3$ are $\int_{\Omega_i} f \, dA$ for $i \in \mathcal{N}_{singular}$.

Owing to the support of the basis functions $\{\phi_j\}_{j=1}^{N_{node}}$, matrix $[A_{31}A_{32}]$ has sparsity structure similar to matrix $[A_{11}A_{12}]$. Matrix A_{23} is usually a dense $N_{bound} \times N_s$ matrix, but the size of this matrix is much smaller than the size of $\hat{A}$. Since $N_s = 2(p+1)-1$, comparing with system (32), the size of system (45) has increased only by $2(p+1)-1$, and the number of non-zeros has increased only by $O(N_{bound}) = O(1/h)$. The total number of non-zeros in $\hat{A}$ remains $O(1/h^2)$. We shall refer to this approximation technique for the solution of the BVP by pth *order augmented FVEM*.

4. Numerical experiments

4.1. Model Problem 1: regular solution

We first consider Model Problem 1 described in Section 2.2. The solution to this BVP is a 9th order polynomial. The H^1 and L_2 errors for our numerical experiments on a regular grid as in Fig. 4 are plotted in Figs. 6 and 7, respectively. As can be seen, the error converges immediately to near machine accuracy for the 9th and 10th order FVEM (i.e., $p = 9, 10$). For other order FVEM, the error converges as follows:

$$\|u - u^h\|_{H^1} = O(h^p), \tag{46}$$

$$\|u - u^h\|_{L_2} = \begin{cases} O(h^{p+1}) & \text{for } p = 1, 3, 5, 7, 8, \\ O(h^p) & \text{for } p = 2, 4, 6, \end{cases} \tag{47}$$

where u is the exact solution of BVP (1)–(2), u^h is the approximation obtained by the FVEM and h is the diameter of the element triangles. This convergence behaviour is similar to what is shown theoretically in [9] for the FVEM applied to one-dimensional problems. It is noteworthy that similar convergence behaviour for the L_2 norm with sub-optimal convergence rates for even polynomial order can also be found for the Discontinuous Galerkin method [19]. To investigate whether this L_2 convergence behaviour may be the result of error cancellation on our regular mesh, we repeated the calculations on slightly perturbed grids with the vertices of element triangles in the interior of the domain randomly relocated within distances of h/10 from their original location. Fig. 8 indicates that the odd–even dichotomy for the L_2 convergence is not due to error cancellation effects on regular grids. It is interesting that for Discontinuous Galerkin methods, the odd–even dichotomy only seems to occur on regular grids [19–21], while we (and others) also observe it on non-regular grids for the FVEM [18].

4.2. Model Problem 2 : singular solution

Second, we consider Model Problem 2 described in Section 2.3. The solution to this BVP has a boundary derivative blow-up singularity (i.e., the r-directional derivative blows up at the origin). We consider the FVEM with the standard trial function space (Section 3.3) first, and then the augmented trial function space (Section 3.4).

4.2.1. FVEM with standard trial function space

As can be seen in Fig. 9 using the high order FVEM with standard trial function space, the rate of convergence does not increase as the order of the method increases. The 1st and 2nd order FVEM appear to converge initially with higher order than the 3rd to 10th order methods. We suspect that this is due to the fact that their errors are initially dominated by the regular part of the solution.

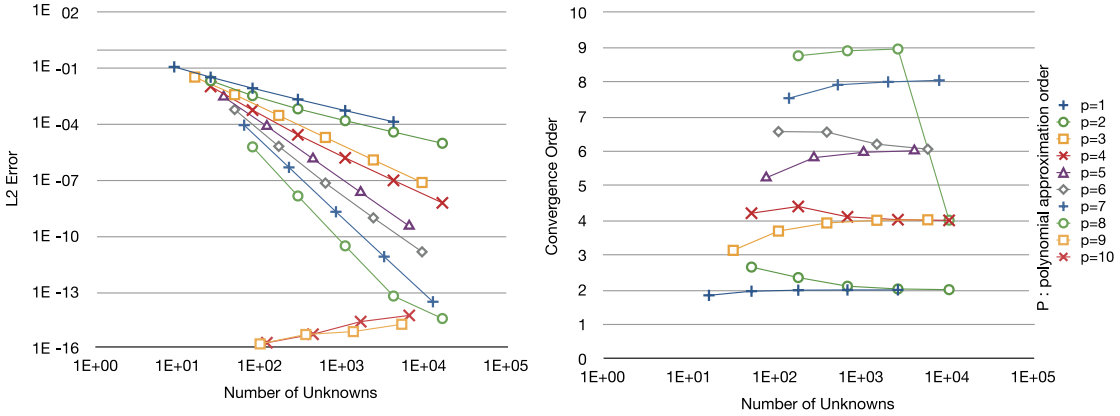

Fig. 7. L_2 error convergence for the Poisson problem with 9th order polynomial exact solution (Model Problem 1).

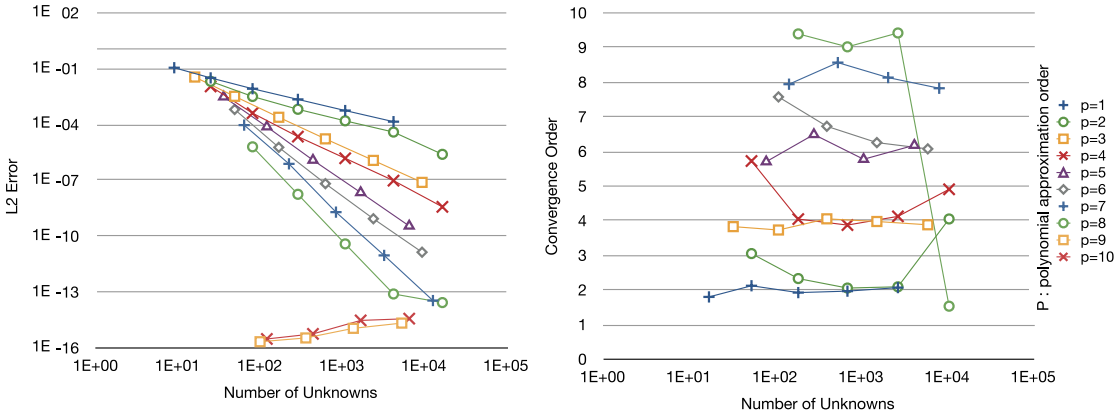

Fig. 8. L_2 error convergence for the Poisson problem with 9th order polynomial exact solution on a randomly perturbed grid (Model Problem 1).

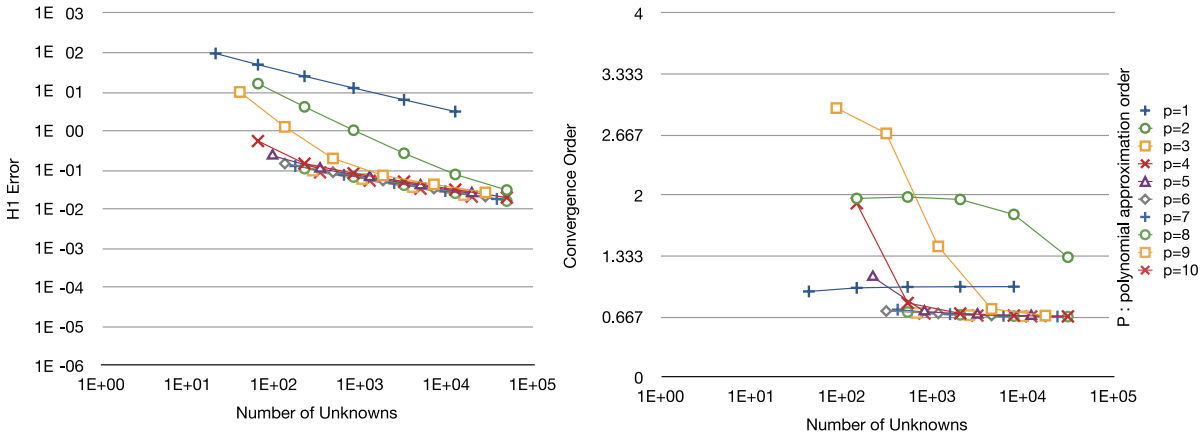

Fig. 9. H^1 error convergence for derivative blow-up singular solution (Model Problem 2).

4.2.2. *FVEM with augmented trial function space*

As can be seen in Fig. 10 using the augmented trial function space, we recover a rate of convergence similar to the smooth case (the BVP with 9th order polynomial solution, Fig. 6). That is to say, the error behaves like in Eq. (46) and high order convergence rates are restored.

5. Conclusion

We have described how the idea of augmentation of the trial function space can be applied to the FVEM, and have presented numerical experiments that indicate that high order convergence rates can be recovered by augmenting the trial function space. Due to the nature of the discrete integral formulation of the FVEM, an augmented FVEM can be constructed in a much simpler way than an augmented FEM. In particular, the singular basis functions only appear in the boundary

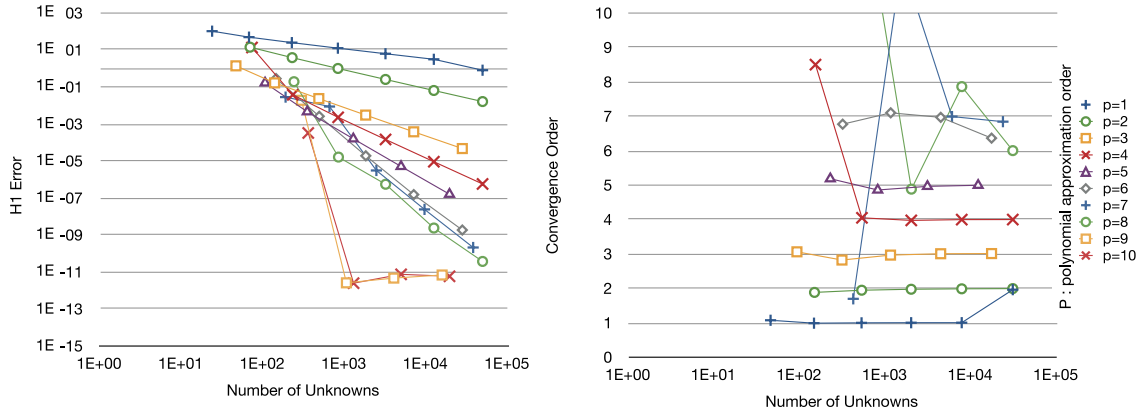

Fig. 10. H^1 error convergence for derivative blow-up singular solution with augmented trial function space (Model Problem 2).

conditions, which leads to the fact that there is no need for singular integration, and that the sparsity of the matrix is automatically maintained.

Due to its simplicity, the high order augmented FVEM we propose may have clear advantages over FEM approaches when approximating the solution of a Poisson problem with singularities. Our findings thus constitute a clear motivation for pursuing theoretical convergence results on the FVEM on triangular grids beyond order 2.

Acknowledgements

The first author would like to thank the National Institute of Informatics in Tokyo, Japan, since this paper was prepared while holding an internship position at the institute. Also, the authors would like to thank NSERC of Canada for supporting this research project. In addition, the authors would like to thank Prof. Norikazu Saito and Dr. Issei Oikawa of the Tokyo University for sharing their knowledge of the Discontinuous Galerkin method.

References

[1] R.E. Bank, D.J. Rose, Some error estimates for the box method, Numer. Anal. 24 (1987) 777–787.
[2] F. Liebau, The finite volume element method with quadratic basis functions, Computing 57 (1996) 281–299.
[3] R. Li, Z. Chen, W. Wu, Generalized Difference Methods for Differential Equations, Marcel Dekker Inc., 2000.
[4] J. Xu, Q. Zou, Analysis of linear and quadratic simplicial finite volume methods for elliptic equations, Numer. Math. 111 (3) (2009) 469–492.
[5] M. Yang, A second-order finite volume element method on quadrilateral meshes for elliptic equations, Math. Model. Numer. Anal. 40 (6) (2007) 1053–1067.
[6] M. Yang, J.N. Liu, C. Chena, Error estimation of a quadratic finite volume method on right quadrangular prism grids, J. Comput. Appl. Math. 229 (1) (2009) 274–282.
[7] L. Chen, A new class of high order finite volume methods for second order elliptic equations, SIAM J. Numer. Anal. 47 (6) (2010) 4021–4042.
[8] Z. Chen, R. Li, A. Zhou, A note on the optimal L^2-estimate of the finite volume element method, Adv. Comput. Math. 16 (4) (2002) 291–303.
[9] M. Plexousakis, G.E. Zouraris, On the construction and analysis of high order locally conservative finite volume type methods for one dimensional elliptic problems, SIAM J. Numer. Anal. 42 (3) (2004) 1226.
[10] P. Grisvard, Elliptic problems in nonsmooth domains, in: Monographs and Studies in Mathematics, Pitman, 1985.
[11] P. Grisvard, Singularities in Boundary Value Problems, Springer-Verlag, 1992.
[12] G. Strang, G.J. Fix, An Analysis of the Finite Element Method, Prentice-Hall, 1973.
[13] P. Chatzipantelidis, R.D. Lazarov, Error estimates for a finite volume element method for elliptic PDEs in nonconvex polygonal domains, SIAM J. Numer. Anal. 42 (5) (2005) 1932.
[14] K. Djadel, S. Nicaise, J. Tabka, Some refined finite volume methods for elliptic problems with corner singularities, J. Numer. Math. 12 (4) (2004) 255.
[15] A. Vogel, Higher order finite volume method for elliptic partial differential equations, in: European Multigrid Conference 2008 (oral presentation), 2008.
[16] Z.J. Wang, Spectral (finite) volume method for conservation laws on unstructured grids. basic formulation: basic formulation, J. Comput. Phys. 179 (2) (2002) 665.
[17] Z.J. Wang, Spectral (finite) volume method for conservation laws on unstructured grids: II. extension to two-dimensional scalar equation, J. Comput. Phys. 178 (1) (2002) 210.
[18] A. Vogel, J. Xu, G. Wittum, A generalization of the vertex-centered finite volume scheme to arbitrary high order, Comput. Vis. Sci. 13 (5) (2010) 221–228.
[19] J.T. Oden, I. Babuska, C.E. Baumann, A discontinuous *hp* finite element method for diffusion problems: 1-D analysis, J. Comput. Phys. 146 (2) (1998) 491–519(29).
[20] M.G. Larson, A.J. Niklasson, Analysis of a family of discontinuous Galerkin methods for elliptic problems: the one dimensional case, Numer. Math. 99 (September) (2004) 113–130.
[21] J. Guzman, B. Riviere, Sub-optimal convergence of non-symmetric discontinuous galerkin methods for odd polynomial approximations, J. Scientific Comput. 40 (2009) 273–280.
[22] S.C. Brenner, L.R. Scott, The Mathematical Theory of Finite Element Methods, in: Texts in Applied Mathematics, vol. 15, Springer, New York, 1994.